Journal of Materials Chemistry A

Accepted Manuscript

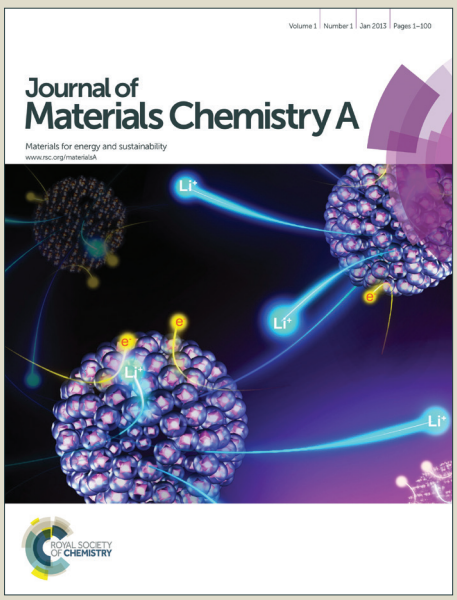

ROYAL SOCIETY OF CHEMISTRY

www.rsc.org/materialsA

Journal of Materials Chemistry A

Dynamic Article Links ►

Cite this: DOI: 10.1039/c0xx00000x

PAPER

www.rsc.org/xxxxxx

Monodispersed hollow platinum nanospheres: facile synthesis and their enhanced electrocatalysis for methanol oxidation

Mianyan Yang, Qixing Cai, Chang Liu, Rui Wu, Dongmei Sun,* Yu Chen, Yawen Tang and Tianhong Lu*

Received (in XXX, XXX) Xth XXXXXXXXX 20XX, Accepted Xth XXXXXXXXX 20XX
DOI: 10.1039/b000000x

Hollow metallic nanospheres with specific composition in different size and shapes have drawn enormous interest due to their strong catalytic activity. In this work, we present an efficient method for facile synthesis of monodispersed Pt hollow nanospheres (Pt-HNSs) using colloidal silica nanoparticles as a sacrificial template. Two steps were involved in the fabrication process. At first, a uniform durable thin layer of anionic $PtCl_6^{2-}$ was grown on a solid surface of freshly-made polyelectrolyte-modified nano-silica, which have evenly-spread positive charges in the outmost surface, as a result of the sequential adsorption in the order of cationic PDDA (Poly(diallyldimethylammonium chloride)), anionic PSS (poly(sodium4-styrenesulfonate)) and PDDA through electrostatic interaction by a layer by layer (LBL) self assembly. Then, the $PtCl_6^{2-}$ species were chemically reduced by $NaBH_4$ in the presence of trisodium citrate dehydrate as a complex agent, followed by the chemically removing of the template. The composition, structural morphology and electrocatalytical properties of the as-prepared Pt-HNSs were thoroughly characterized by techniques, such as high-resolution transmission electron microscopy (HRTEM), field emission scanning electron microscopy (FESEM), X-ray diffraction (XRD), and cyclic voltammetry (CV). The results show that the as-prepared well-dispersed Pt-HNSs with narrow size distribution, exhibit significant catalytic activity to the oxidation of methanol, when compared with that of commercial Pt-black.

1. Introduction

Direct methanol fuel cells (DMFCs), an important alternative green-energy system, predominant in portable power and automotive applications, have attracted extensive attention during the past two decades due to its simplicity, near-zero emission of pollutants, low operating temperatures, and high theoretical efficiency of energy conversion.[1-6] However, for large-scale commercialization, there are still several technical hurdles remained to be overcome for DMFCs.[7] One of the challenges with the anode electrocatalyst is the limited utilization efficiency of the leading catalyst materials of noble Pt,[8, 9] which is of high cost and low abundance. Another challenge is the poor kinetics of the anodic oxidation of methanol by Pt due to the strong binding of intermediate CO species to the active sites.[10] Therefore, the development of high performance anode catalysts with enhanced activity, stability and using efficiency are the key issues for the development of DMFCs.[11]

Much efforts has been made to achieve better utilization of Pt catalysts with enhanced electrocatalytic activity, by such as shaping in nanoparticles, nanowrires, or nanotubes, combining with less expensive/more aboundant metals or dispersing on the surface of suitable support.[12-15] In particular, the hollow metal spheres possess some of prominent advantages over their solid counterparts. First, the hollow structure geometry endows them with beneficial properties of low density, high surface area, and extra interior reaction space leading to an increase in the reaction rate due to the confinement of the cage effect, as shown in the previous report on different hollow metallic nanopheres.[16-18] It is reported[19, 20] that the confinement effects causing catalytic enhancement is affected by the cavity size inside the cage, which at appropriate range, acting as a nanoreactor, will allow for an optimum collision rate between the reactants, resulting in high electrocatalytic activity due to increased attempt frequencies and improved kinetics. In the mixed kinetic- and diffusion-limited region, the reaction rate constant decreased or leveled off as the size of the cages increases after the cage size went beyond a maximum value. Within a certain range, the electrocatalytic activity was found to increase with porous depths, which could reach as high as approximately 200 nm[20]. Second, the porous submicrometer-sized hollow spheres, which shell consists of firmly intra-connected metal nanoparticles, can provide large quantity of catalytic sites, meanwhile, avoid the aggregation of small catalyst particles, which is a common problem facing substrate-supported metal catalysts. Until now, there have been

some reports on hollow metal spheres. Cheng and his coauthors[21] reported that $Ni_{1-x}Pt_x$ (x = 0 - 0.12) hollow sphere was a catalyst with high electrocatalytic performance for ammonia borane. Sang-wok Kim etc reported[18] the successful fabrication of hollow palladium spheres and their application as a recyclable heterogeneous catalyst for Suzuki coupling reactions. Vasquez etc prepared[16] hollow CoPt nanopheres through a novel one-pot reaction using an in situ sacrificial template. There are several different synthetic methods to produce hollow metal nanospheres,[22-25] such as template-mediated techniques, metal diffusion based on the Kirkendall effect, and the galvanic replacement method. Typically, Dubau and his coauthors[22] present "hollow" Pt nanoparticles grown from dealloying fresh Pt_3Co alloy induced by Kirkendall effect. However, the relatively densely-packed shell of the obtained hollow Pt nanoparticles might not be beneficial for the reactants and products to diffuse into and out of the cavity, which is one of the crucial factors for common high confinement behavior as reported. Bai group[23] provides an efficient protocol for facile synthesis of Pt hollow nanosphere using Co nanoparticle as a sacrificial template. But, it is well-known that cobalt itself is expensive and toxic. Additionally, nitrogen was bubbled through the solution during the whole procedure, which made the fabrication process relatively complicated and expensive. For sacrificial template-directed fabrication, the most commonly used template is polymer beads or SiO_2 spheres, which define the shape and size of the resulting nanoshells, generally deposited through layer-by-layer self-assembly[26] or electroless deposition.[27] The layer-by-layer (LBL) approach has been developed to synthesize uniform CNT-metal nanocomposites at room temperature. For example, Du etc reported[28] a general approach for fabrication of CNT-Pt, CNT-Pd, and CNT-Sn nanocomposites, by layer-by-layer assembly, with evenly-distributed thin metal layer deposited on the outside surface of MWCNTs, which motivates us to have the basic idea presented here.

In this paper, we use polyelectrolyte-modified colloidal silica with evenly spread positive charges on the outside surface, as a sacrificial template for the controllable electrostatic adsorption of a thin uniform layer of noble metal ions to fabricate monodispersed hollow metallic nanospheres. The positively charged silica could strongly adsorb the negatively charged metal ions, such as $PtCl_6^{2-}$, $PdCl_4^{2-}$, or BH_4^-, which ensured that the reduction reaction took place on the surface of the silica spheres. $NaBH_4$ and trisodium citrate dehydrate were chosen as the reducing agent and complex agent, respectively, to produce uniform metal nanoparticles from metal salt on the polyelectrolyte-modified SiO_2 under sonication. When $PtCl_6^{2-}$ was selected as a model ion, after complete removal of the template, hollow platinum nanospheres (Pt-HNSs) were successfully produced. The obtained hollow catalysts of Pt-HNSs present high electrocatalytic activity and good stability to the electrooxidation of methanol, compared with that of commercial Pt black as demonstrated as follows. This method we present here, can be easily extended to synthesize hollow nanospheres of different metals and composition.

2. Experimental

2.1 Reagents and chemicals

H_2PtCl_6 was purchased form Snopharm Chemical Reagent Co., Ltds. (Shanghai, China). Poly (diallyldimethylammonium hloride) (PDDA, Mw < 500000 Da), and poly (sodium 4-styrenesulfonate) (PSS, Mw < 700000 Da), were purchased from Alfa Aesar Co. Ltd. All other chemicals were commercially available and of analytical grade. All reagents and chemicals were used without further purification. The deionized water from a Milli-Q Millipore (Bedford, MA, USA) purification system at a resistivity of > 18.0 MΩ/cm was used throughout the experiments.

2.2 Pt-HNSs catalysts preparation

Monodispersed SiO_2 spheres were synthesized using the method of tetraethyl orthosilicate (TEOS) hydrolyzation in alkaline condition as reported previously with minor modification. Typically, a total of 100 mL ethanol, 6 mL H_2O, 6 mL ammonium hydroxide, 3 mL TEOS were mixed and stirred for 5 hours, then the resulting suspension was filtered, washed for several times with water and dried in oven at 80 °C, resulting in monodispersed SiO_2 nanospheres. The obtained SiO_2 nanospheres were used as a template to produce Pt-HNSs. In detail, 0.5g of freshly-made SiO_2 was sonicated in 60 mL of 0.5 M NaCl solution for 1 h, and then 0.75 g of PDDA was added. The mixture mentioned above was stirred for 1 h. After that, the excess PDDA was removed by five repeated centrifugation/wash cycles. Similarly, the PSS and PDDA layers were then sequentially coated on the surface of the PDDA-modified SiO_2 for PDDA/PSS/PDDA-modified SiO_2. To obtain uniform SiO_2-Pt nanocomposites, 30 mg of the polyelectrolyte-modified SiO_2 was put into 40 mL of water with 30 mg of H_2PtCl_6 and 60 mg of trisodium citrate dehydrate, which were sonicated for 30 min. $NaBH_4$ (10 mg) aqueous solution was then slowly dropped into the above-metioned solution under mild sonication. After 1 h, the resulting black solid products were centrifugalized, washed with distilled water and ethanol, respectively, to remove the unreacted metal ions possibly remained in the final solution, then dried at 50 °C in air. The as-prepared Pt/SiO_2 was put into 2 M NaOH solution for 24 h, followed by centrifuging, washing with distilled water and ethanol, and dried in a vacuum oven at 50 °C, to obtain hollow Pt nanospheres.

2.3 Physical characterization

The composition of the catalysts was determined using the energy dispersive spectrum (EDS) technique with Vantage Digital Acquisition Engine (Thermo Noran, USA). The X-ray diffraction (XRD) measurements were performed on Model D/max-rC diffractometer using Cu Ka radiation (λ = 0.15406 nm) operating at 45 kV and 100 mA. Transmission electron microscopy (TEM) was carried out using a JEOL JEM-2100F transmission electron microscope operating at 200 kV with the nominal resolution. Scanning electron microscopy (SEM) images were captured on a JSM-2010 microscopy at an accelerating voltage of 20 kV. Energy dispersive X-ray (EDX) analysis was carried out on a JEOL JSM-7600F SEM.

2.4 Electrochemical measurement

The electrochemical measurements were carried out at 30±1°C with a CHI600 electrochemical analyzer (CHI instruments Co., USA) and a conventional three electrode electrochemical cell. A

Pt plate was used as the auxiliary electrode. The saturated calomel electrode (SCE) was used as the reference electrode. All the potentials were quoted with respect to SCE.

The working electrodes were prepared as follows. A glassy carbon electrode was polished sequentially with 0.3 and 0.05 μm Al_2O_3, followed by a wash with water/ethanol via sonication after each step. Then, 2 mg as-prepared Pt-HNSs catalysts and 1 mL H_2O were thoroughly mixed to produce a catalyst slurry blend. Next, 8.9 μL of the obtained slurry was spread on the surface of the pretreated GCE. After drying, 3 μL Nafion (5 wt %) solution was used to cover the surface of the catalyst layer. The diameter of the glassy carbon electrode is 4 mm and the geometric surface area is 0.1256 cm^2. The specific loading of the catalyst on the electrode surface was 28 μg cm^{-2}. The electrolyte is 0.5 M H_2SO_4 solution with or without 0.5 M CH_3OH. Prior to the measurements, a steady stream of N_2 was bubbled into the solution for 10 min to remove O_2 in the electrolyte. During the measurement, N_2 was flowed above the solution. Adsorption of CO was performed by immersing the electrode into and bubbling CO through the solution for 15 min at a potential of 0 V. After adsorption, CO was purged from solution by N_2 bubbling for 10 min.

3. Results and discussion

3.1 Characterization of Pt-HNSs Catalysts

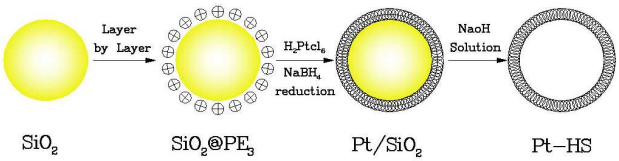

Scheme 1 Schematic illustration of the fabrication procedure to produce Pt hollow nanospheres.

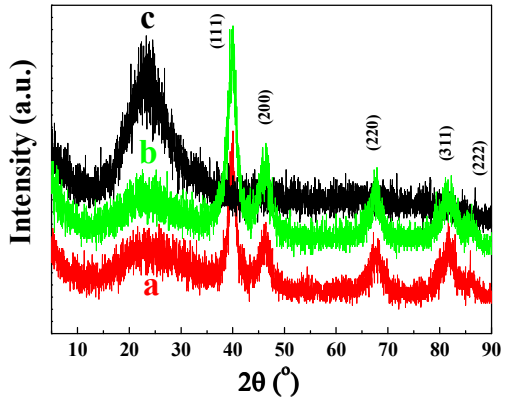

Fig. 1 The XRD patterns of (a) Pt hollow nanospheres, (b) Pt/SiO_2 and (c) SiO_2.

Colloidal silica nanosphere with narrow diameter distribution was selected, in particular, as a sacrificial matrix for fabrication of Pt-HNSs, because of its desirable morphology, ease to be made and relative high stability. The schematic illustration of the preparation procedure was demonstrated in scheme 1.

Fig. 1 shows the typical XRD patterns of the prepared nanospheres. As observed in Fig. 1a and 1b, there are five diffraction peaks located at 39.76°, 46.24°, 67.45°, 81.28° and 85.71°, which can be indexed to (111), (200), (220), (311) and (222) planes of face-centered cubic (fcc) crystalline Pt, respectively (JCPDS standard 05-0681(Pt)). By contrast, no any characteristic peaks of Pt were observed in Fig. 1c for SiO_2. These results indicate that the proposed protocol as mentioned above, is efficient, enabling the formation of uniform Pt-HNSs, which will be further demonstrated in the following by TEM and SEM as well. In addition, the broadening of diffraction peaks, mainly caused due to the smaller average grain size, reveals that Pt-HNSs might be composed of many small crystals.

Fig. 2 represents TEM/SEM images of SiO_2, Pt/SiO_2 and Pt-HNSs particles. As shown in Fig. 2A and 2B, the SiO_2 particles possess a similar size of ca. 200 nm. Images of Pt/SiO_2 as shown in Fig. 2C and 2D, confirm that, when Pt was sequentially deposited on the surface of polyelectrolyte-modified SiO_2 nanoparticles, the surface becomes less smooth and rougher without obvious morphology change. The SEM images of Pt-HNSs catalysts in Fig. 2E, reveal a spherical structure. The white arrows highlight some of broken hollow nanospheres, from which it is clear that the inner space in the as-prepared Pt-HNSs was vacant indicating that the template of SiO_2 was removed, leading to a hollow structure. The TEM images of Pt-HNSs in Fig. 2F, display that the as-prepared hollow platinum spheres have similar morphology to that of the selected template with a diameter around 200 nm, indicating that the structural integrity is basically maintained after the incorporation of the Pt nanoparticles and the removing of the template. These observations demonstrate Pt-HNSs, robust replicas of the template particles, can be fabricated successfully using the procedure shown in Scheme 1.

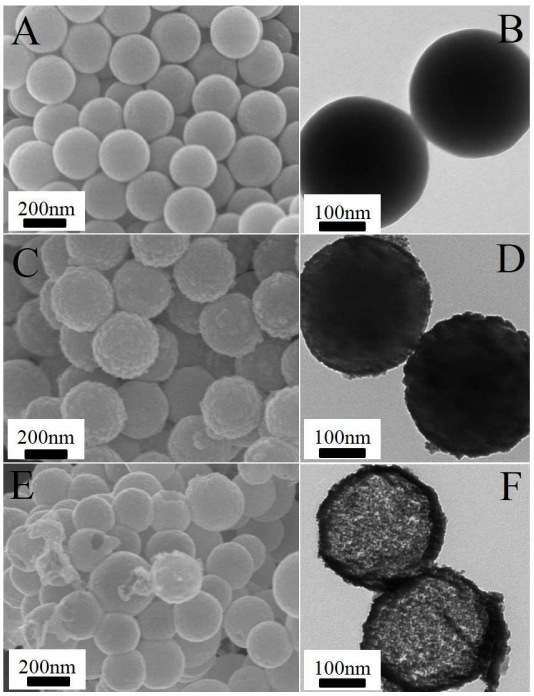

Fig. 2 SEM images (A, C, E) and low resolution TEM images (B, D, F) of SiO_2 (A, B), Pt/SiO_2 (C, D) and Pt-HNSs (E, F).

To further characterize the as-prepared Pt-HNSs, more experiments were conducted. As shown in Fig.3A and 3B, the structural integrity of most produced double-shelled hollow Pt with narrow distributed size was preserved even after sonication over relatively long periods of time, indicating good mechanical properties of the as-prepared Pt-HNSs. The SEM image (inset, Fig. 3B) of a destructed fragment of Pt-HNSs confirms the hollow structure as well. In Fig. 3C and 3E, the enlarged TEM image of an individual Pt-HNS clearly shows the inner and outer surfaces of hollow spheres, on which the building block, Pt nanoparticles are well dispersed, and actually interconnected through shared outside surface. According to the histogram of Pt particle size distribution (inset, Fig. 3C), the diameter of Pt nanoparticles on the surface of SiO_2 is about 4.7 nm, in accordance to the result from XRD data analysis. High angle annular dark field (HAADF) scanning transmission electron microscopy (STEM), HAADF-STEM image (image a, Fig. 3D) and EDX elemental mapping pattern (image b, Fig. 3D) indicate the homogenous distribution of Pt nanoparticles on the hollow sphere as well. EDX line scan (curve e, Fig. 3D) analysis reveals the Pt profile through one single Pt-HNS, confirming the hollow structure. Moreover, the magnified high resolution TEM (HRTEM) image in Fig. 3D, image c and d show the Pt-HNSs have steps and high-index facets exposed. It is expected that Pt-based catalysts with such structure generally exhibit improved electrocatalytic activity for corresponding electrocatalytic reaction. The interplanar spacing of 0.232 nm is observed on Pt-HNSs surface as shown in Fig. 3F, which corresponds to the distance between (111) lattice planes of the face-centered cubic crystalline Pt.

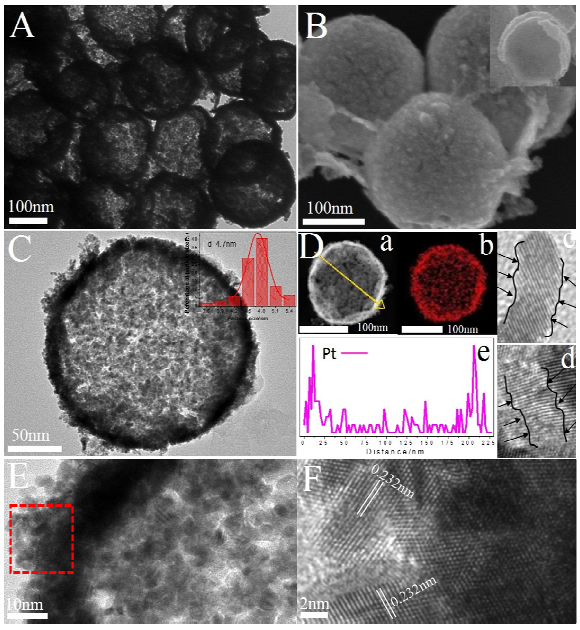

Fig. 3 Morphological and structural characterizations of as-prepared Pt-HNSs: (A,C, E) TEM images, (B) SEM image, inset: SEM image of a destructed fragment, (image a, D) HAADF-STEM image, (image b, D) EDX elemental mapping patterns, (image e, D) EDX line scanning analysis, (image c, d, D) the lattice fringe image of low-coordinated defective atoms, and (F) HRTEM image of the squared area bordered by a dashed red line in image E.

3.2 Electrocatalytic performance of as-prepared Pt-HNSs modified GC electrode

Fig.4A shows the cyclic voltammograms (CV) of the Pt-HNSs/GC and Pt black/GC electrodes in 0.5M H_2SO_4 solution at a scan rate of 50 mV s^{-1}. It can be clearly observed that the voltammograms of these two Pt-based catalyst-modified electrodes display normal features characteristic of hydrogen and oxygen adsorption/desorption, typical for polycrystalline Pt, whether in anodic or cathodic sweep. The peak at higher potential of 0.5 V is attributed to the reduction of the Pt oxide formed on the surface of Pt-HNSs during the forward scan. Meanwhile, characteristic peaks in lower potential region from -0.2 V to 0.1 V, are attributed to atomic hydrogen adsorption/desorption on the Pt surface and reflect the number of Pt sites that are available for hydrogen adsorption and desorption.[29, 30] The electrochemically active surface area (ECSA) of the Pt catalysts can be estimated by integrating cathodic/anodic current in the hydrogen adsorption/desorption region of the cyclic voltammogram. The ECSA value (A) can be obtained from the following equation $A = Q_H/0.21$ mC cm^{-2}, where 0.21 mC cm^{-2} is the characteristic value of charge density associated with a monolayer of hydrogen adsorbed on polycrystalline platinum.[31-33] The calculated ECSA value of the as-prepared Pt-HNSs/GC electrode is 19.66 m^2/g, which is 1.57 times larger than that of Pt black. This implies that Pt-HNSs can distinctly improve the accessibility of reactants to the electrochemically active sites of Pt.

Superior poison tolerance of Pt hollow spheres was directly confirmed by CO_{ads}-stripping analysis as shown in Fig. 4B. The onset potential and peak potential of CO_{ads} oxidation on Pt-HNSs negatively shift ca.120 and 19 mV, respectively, compared to those on Pt black. Meanwhile, according to the equation ECSA = Q_{CO}/q (q = 0.42 mC cm^{-2}), where Q_{CO} is the total charge for the oxidation of CO.[34] The calculated charges for the oxidation of CO at the Pt-HNSs and Pt black catalyst modified electrodes are 9.807×10^{-4} C and 8.324×10^{-4} C respectively, thus the corresponding ECSA value are 2.335 cm^2 and 1.982 cm^2, respectively, indicating CO adsorption on Pt-HNSs surface is weaker than it is on Pt black. These results indicate that the special hollow morphology of as-prepared Pt-HNSs makes it possible to improve the CO tolerance of the electrocatalysts.

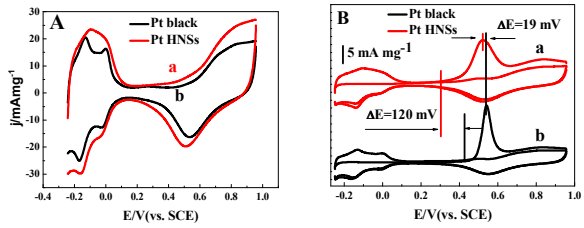

Fig. 4 (A) CV curves of (a) Pt-HNSs and (b) commercial Pt black in N_2-saturated 0.5 M H_2SO_4 solution at a scan rate of 50 mV s^{-1}. The ECSA of Pt electrocatalyst was calculated by measuring the charge collected in the hydrogen adsorption/desorption region after double-layer correction. (B) CV curves of pre-adsorbed CO at (a) Pt-HNSs and (b) commercial Pt black in 0.5 M H_2SO_4 solution at the scan rate of 50 mV s^{-1}.

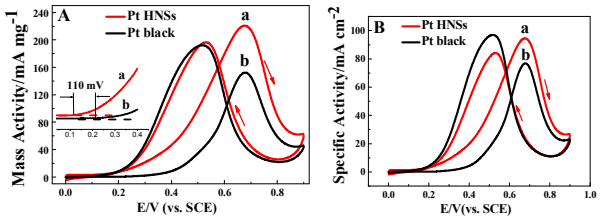

Fig. 5 CV curves of (a) Pt-HNSs and (b) commercial Pt black in N_2-saturated 0.5 M H_2SO_4 with 1.0 M CH_3OH solution at a scan rate of 50 mV s^{-1}, which are normalized to (A) Pt mass (mass activity) and (B) the real Pt ECSA (specific activity), respectively. Arrows indicate the potential scan direction.

Methanol was selected as a model molecule for studying the electrocatalytic activity of Pt-HNSs because of its important application in direct methanol fuel cells (DMFCs). The mass activity of electrocatalysts (i.e., the currents are normalized to the metal mass) is generally taken as an index to assess the applicability of electrocatalysts. The electrocatalytic properties of Pt-HNSs and commercial Pt black for methanol oxidation reaction (MOR) were firstly investigated by CV, under the same Pt loading (Fig. 5A). Two obvious anodic peaks (i.e., methanol oxidation peak at higher potential and intermediate carbonaceous species oxidation peak at lower potential), typical for methanol electrooxidation, are observed on both Pt-HNSs and Pt black based electrodes during the positive and negative scan directions. However, compared to Pt black, the onset oxidation potential and oxidation peak potential of methanol on Pt-HNSs/GC negatively shift ca. 110 and 1 mV, respectively, which result in a large enhancement in electrocatalytic activity. For example, the methanol oxidation current at 0.5 V (a typical working potential for DMFCs) are 99.3 and 34.5 mA mg^{-1} on Pt-HNSs and Pt black, respectively. Obviously, the electrocatalytic activity of Pt-HNSs has been enhanced remarkably at this potential compared to that of Pt black, indicating Pt-HNSs hold promise as a potential practical electrocatalyst for methanol oxidation. Besides the mass activity for evaluating the effectiveness of Pt utilization, the specific activity (i.e., the current are normalized to ECSA of metal electrocatalysts) is another commonly used parameter to evaluate the actual value of the intrinsic activity of the electrocatalysts. Thus, the electrocatalytic properties of Pt-HNSs and commercial Pt black for the MOR were further studied along this line by CV as well, under the same ECSA value (Fig. 5B). As observed, specific current density of methanol oxidation on Pt-HNSs/GCE (42.5 mA cm^{-2}) is 2.4 times higher than that on commercially available Pt black/GCE (17.4 mA cm^{-2}) at 0.5V, further confirming that Pt-HNSs have better electrocatalytic activity than Pt black. During the MOR, Pt-based electrocatalysts easily lose a large amount of activity owing to the poisoning adsorption of CO_{ads} and/or unidentified non-CO_{ads} organic species. The current ratio of the forward oxidation (I_f) to the reverse oxidation (I_b), I_f/ I_b, can be used to evaluate the tolerance of the catalysts to poisoning.[35] High I_f/I_b ratio indicates more effective removal of poisoning species from the catalysts' surface. For Pt-HNSs, the I_f/I_b ratio is 1.12, which is much higher than 0.79 for commercial Pt black, demonstrating better tolerance to CO of Pt-HNSs than of Pt black. In addition, the as-prepared Pt-HNSs hold better tolerance to CO than that of the one[36] reported, previously, with shells composed of interconnected Pt nanowires (2 nm in diameter), which was prepared using SiO_2 as sacrificial template as well, though different surface modification for silica spheres by silanation using silane-coupling agents of aminopropyltriethoxysilane (APTES) in organic solvent of tetrahydrofuran (THF) was applied, in which toxic and flammable THF and toxic APTES, have to be employed unavoidably.

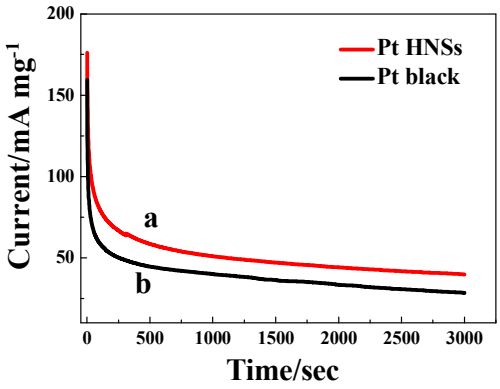

Fig. 6 Chronoamperometry curves of (a) Pt-HNSs and (b) commercial Pt black in 0.5 M H_2SO_4 solution with 0.5 M CH_3OH for 3000 s at 0.66 V.

The electrocatalytic activity and durability of Pt-HNSs and Pt black for MOR were further investigated by chronoamperometry at 0.5 V potential as shown in Fig. 6. During the whole reaction process, methanol oxidation current on Pt-HNSs is higher than that on commercial Pt black, further confirming that the electrocatalytic activity of Pt-HNSs are better than that of Pt black. The enhanced electrocatalytic activity of Pt-HNSs catalyst might be ascribed to the confinement of the cage effect, their sufficient active sites, the small size of interconnected nanoparticles, and high density of active low-coordinated defective atoms on nanoshell surface such as edge, corner, and surface stepped atoms. At 3000 s, methanol oxidation currents on Pt-HNSs and Pt black decrease to 31.59% and 35.13% of their initial value (taken at 20 s to avoid the contribution of the double-layer discharge and hydrogen adsorption).

4. Conclusions

In summary, Pt hollow nanospheres were prepared by LBL assembly using monodispersed silica particles modified by charged polyelectrolye as a template. The strong electrostatic attraction between metal salts of $PtCl_6^{2-}$ and polyelectrolyte-modified SiO_2 spheres, the appropriate reduction and growth rate, and the sonication treatment play an important role in the homogeneous deposition of well-attached metal layers on solid SiO_2 spheres. It was found that the electrocatalytic performance and long-term durability of the prepared Pt hollow nanospheres as an electrocatalyst is much better than that of the Pt commercial black for methanol oxidation reaction. The excellent electrocatalytic performance of Pt-HNSs could be probably attributed to the specific hollow porous nanostructure with small-sized platinum nanoparticles innerconnected with each other on the surface, providing sufficient active sites and high density of active low-coordinated defective atoms. The presented Pt-HNSs

with superior electrocatalytic performance hold promise as an efficient anode electrocatalyst for the application in DMFCs.

Acknowledgements

The authors thank the financial support from the National Natural Science Foundation of China (21376122, 21273116), National "973" program of China (2012CB215500), the Natural Science Foundation of Jiangsu Province (BK20131395), the United Fund of NSFC and Yunnan Province (U1137602), the Industry–Academia Cooperation Innovation Fund Project of Jiangsu Province (BY2012001), and Natural Science Foundation of Colleges and Universities in Jiangsu Province (10KJB150007), the Project (No. Y207K5) supported by Key Laboratory of Renewable Energy, Chinese Academy of Sciences and the Project Funded by the Priority Academic Program Development (PAPD) of Jiangsu Higher Education Institutions.

Notes and references

Jiangsu Key Laboratory of New Power Batteries, Jiangsu Collaborative Innovation Center of Biomedical Functional Materials, Jiangsu Key Laboratory of Biofunctional Materials, College of Chemistry and Materials Science, Nanjing Normal University, Nanjing 210023, P.R.China. Fax: +86 25 83243286; Tel: +86 25 85891651; E-mail: sundongmei@njnu.edu.cn, tianhonglu@263.net

1. Z. Wang, G. Gao, H. Zhu, Z. Sun, H. Liu and X. Zhao, *Int. J. Hydrogen Energy*, 2009, **34**, 9334-9340.
2. W. Li, Q. Xin and Y. Yan, *Int. J. Hydrogen Energy*, 2010, **35**, 2530-2538.
3. N. Krishnan, J. Prabhuram, Y. Hong, H.-J. Kim, K. Yoon, H.-Y. Ha, T.-H. Lim and S.-K. Kim, *Int. J. Hydrogen Energy*, 2010, **35**, 5647-5655.
4. D. B. Kim, H.-J. Chun, Y. K. Lee, H.-H. Kwon and H.-I. Lee, *Int. J. Hydrogen Energy*, 2010, **35**, 313-320.
5. H.-J. Chun, D. B. Kim, D.-H. Lim, W.-D. Lee and H.-I. Lee, *Int. J. Hydrogen Energy*, 2010, **35**, 6399-6408.
6. S. Patra and N. Munichandraiah, *Langmuir*, 2008, **25**, 1732-1738.
7. P. Liu, G.-P. Yin and C.-Y. Du, *Electrochem. Commun.*, 2008, **10**, 1471-1473.
8. Y. Qiao and C. M. Li, *J. Mater. Chem.*, 2011, **21**, 4027-4036.
9. Y. Zhou, K. Neyerlin, T. S. Olson, S. Pylypenko, J. Bult, H. N. Dinh, T. Gennett, Z. Shao and R. O'Hayre, *Energ. Environ. Sci.*, 2010, **3**, 1437-1446.
10. J. Xu, X. Liu, Y. Chen, Y. Zhou, T. Lu and Y. Tang, *J. Mater. Chem.*, 2012, **22**, 23659-23667.
11. Z. Yan, G. He, P. K. Shen, Z. Luo, J. Xie and M. Chen, *J. Mater. Chem. A*, 2014, 2, 4014-4022
12. S. Du, *J. Power Sources*, 2010, **195**, 289-292.
13. C. Koenigsmann and S. S. Wong, *Energ. Environ. Sci.*, 2011, **4**, 1161-1176.
14. R. Lv, T. Cui, M. S. Jun, Q. Zhang, A. Cao, D. S. Su, Z. Zhang, S. H. Yoon, J. Miyawaki and I. Mochida, *Adv. Funct. Mater.*, 2011, **21**, 999-1006.
15. B. Xiong, Y. Zhou, R. O'Hayre and Z. Shao, *Appl. Surf. Sci.*, 2013, 266, 433-439
16. Y. Vasquez, A. K. Sra and R. E. Schaak, *J. Am. Chem. Soc.*, 2005, **127**, 12504-12505.
17. Y. Sun and Y. Xia, *Science*, 2002, **298**, 2176-2179.
18. S.-W. Kim, M. Kim, W. Y. Lee and T. Hyeon, *J. Am. Chem. Soc.*, 2002, **124**, 7642-7643.
19. C. Yen, M. Mahmoud and M. El-Sayed, *J. Phys. Chem. A*, 2009, **113**, 4340-4345.
20. J. Snyder, I. McCue, K. Livi and J. Erlebacher, *J. Am. Chem. Soc.*, 2012, **134**, 8633-8645.
21. F. Cheng, H. Ma, Y. Li and J. Chen, *Inorg. chem.*, 2007, **46**, 788-794.
22. L. Dubau, J. Durst, F. Maillard, L. Guétaz, M. Chatenet, J. André and E. Rossinot, *Electrochim. Acta*, 2011, **56**, 10658-10667.
23. H. P. Liang, H. M. Zhang, J. S. Hu, Y. G. Guo, L. J. Wan and C. L. Bai, *Angew. Chem.*, 2004, **116**, 1566-1569.
24. F. Bai, Z. Sun, H. Wu, R. E. Haddad, X. Xiao and H. Fan, *Nano lett.*, 2011, **11**, 3759-3762.
25. Y. Zhong, Z. Wang, R. Zhang, F. Bai, H. Wu, R. Haddad and H. Fan, *ACS nano*, 2014, **8**, 827-833.
26. X. Sun and Y. Li, *Angew. Chem. Int. Ed.*, 2004, **43**, 3827-3831.
27. J. Liu, W. Dong, P. Zhan, S. Wang, J. Zhang and Z. Wang, *Langmuir*, 2005, **21**, 1683-1686.
28. N. Du, H. Zhang, P. Wu, J. Yu and D. Yang, *J. Phys. Chem. C*, 2009, **113**, 17387-17391.
29. A. Leela Mohana Reddy and S. Ramaprabhu, *J. Phys. Chem. C*, 2007, **111**, 16138-16146.
30. L. Li and Y. Xing, *J. Phys. Chem. C*, 2007, **111**, 2803-2808.
31. Y.-J. Gu and W.-T. Wong, *Langmuir*, 2006, **22**, 11447-11452.
32. H. Li, G. Sun, Y. Gao, Q. Jiang, Z. Jia and Q. Xin, *J. Phys. Chem. C*, 2007, **111**, 15192-15200.
33. S. Wei, D. Wu, X. Shang and R. Fu, *Energy Fuels*, 2009, **23**, 908-911.
34. L. Shen, H. Li, L. Lu, Y. Luo, Y. Tang, Y. Chen and T. Lu, *Electrochim. Acta*, 2013, 89, 497-502.
35. L. Wang, M. Imura and Y. Yamauchi, *ACS Appl. Mater. Interfaces*, 2012, **4**, 2865-2869.
36. H. Ataee-Esfahani, Y. Nemoto, L. Wang and Y. Yamauchi, *Chem. Commun.*, 2011, **47**, 3885-3887.

Graphic Abstract

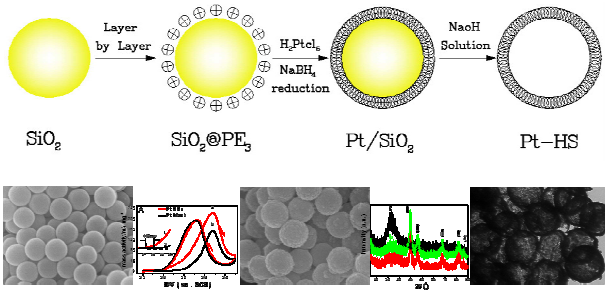

Platinum hollow nanospheres, produced using polyelectrolyte-grafted SiO_2 spheres as a sacrificial template through appropriate reduction of pre-adsorbed $PtCl_6^{2-}$ ions, exhibit markedly enhanced electrocatalytic activity for methanol oxidation toward DMFC applications.